

---

# LOSSLESS COMPRESSION FOR LLM TENSOR INCREMENTAL SNAPSHOTS

---

Daniel G. Waddington  
IBM Research,  
Almaden Research Center, CA, USA

Cornel Constantinescu  
IBM Research,  
Almaden Research Center, CA, USA

June 2024

## ABSTRACT

During the training of Large Language Models (LLMs), tensor data is periodically "checkpointed" to persistent storage to allow recovery of work done in the event of failure. The volume of data that must be copied during each checkpoint, even when using reduced-precision representations such as `bf16`, often reaches hundreds of gigabytes. Furthermore, the data must be moved across a network and written to a storage system before the next epoch occurs.

With a view to ultimately building an optimized checkpointing solution, this paper presents experimental analysis of checkpoint data used to derive a design that maximizes the use of *lossless* compression to reduce the volume of data. We examine how tensor data and its compressibility evolve during model training and evaluate the efficacy of existing common off-the-shelf general purpose compression engines combined with known data optimization techniques such as byte-grouping and incremental delta compression.

Leveraging our analysis we have built an effective compression solution, known as Language Model Compressor (LMC), which is based on byte-grouping and Huffman encoding. LMC offers more compression performance than the best alternative (BZ2) but with an order-of-magnitude reduction in the time needed to perform the compression. We show that a 16-core parallel implementation of LMC can attain compression and decompression throughput of 2.78 GiB/s and 3.76 GiB/s respectively. This increase in performance ultimately reduces the CPU resources needed and provides more time to copy the data to the storage system before the next epoch thus allowing for higher-frequency checkpoints.

## 1 Introduction

Today, LLMs are typically fine-tuned from existing base models. To create the base model a compute and data-intensive *pre-training* phase is needed. This phase uses vast input data sets (e.g., web crawls) to effectively extract language and subject understanding. For large models, such pre-training can take weeks or even months to complete. For example, the BLOOM 176B parameter model (based on GPT3 [9]) took 3.5 months to train on a cluster of 384 80G A100 NVIDIA GPUs with a data set of 350B tokens [16]. At this scale of compute, failures invariably occur ([10] report that failures can slow down training by up to 43%). Prior work has shown that infrastructure and process failures are common in large-scale big data clusters, with a mean time between failure (MTBF) of 4–22 hours [6, 4]. Consequently, resulting outages and restarts can become very costly.

Scale-out of the training means that the compute and data are distributed across a cluster of compute nodes. Parallelism is achieved either distributing the training pipeline or by distributing the model weights and biases through *sharding*. The size of the checkpointed data depends on the model and training scheme. Nevertheless, a single checkpoint, combining data from all nodes, can reach many gigabytes. For example BLOOM checkpoints are 329 GiB in size consisting of data sharded across 48 nodes and 384 GPUs [16]. As the training occurs the tensors are updated over time (see Figure 1).

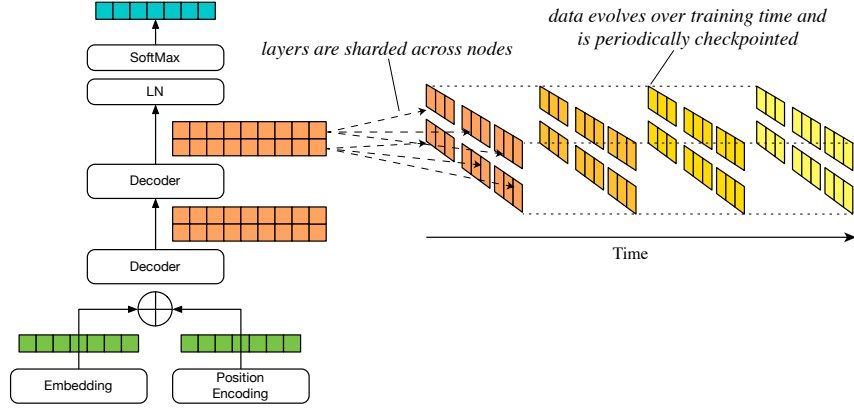


Figure 1: Tensor Data Shards Evolving

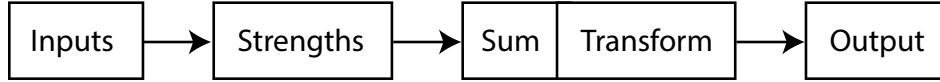


Figure 2: Functional description of a biological neuron's structure [5]

To reduce cost incurred by restarting due to failure in the cluster, *checkpointing* is commonly used. Checkpointing periodically creates a snapshot of GPU memory state at a single point in time. Checkpoints are coherent across multiple nodes in the compute cluster - this is normally achieved by suspending compute at a specified epoch<sup>1</sup>. Once the state has been copied from the GPU memory (e.g., into local host memory) the training workload can asynchronously continue while the checkpoint data is written out to persistent storage.

There is a balance between checkpointing frequency, the volume of data to persist, the time the GPUs are waiting idle, and the time to recover after failure. Prior work focuses on various optimizations of checkpoint frequency, reducing GPU idle time and minimizing recovery time [11, 13, 15].

This paper focuses on reducing the volume of data through lossless compression and the resources and time needed to perform it. We focus on lossless compression so as to allow precise recovery and elimination of unexpected possible side-effects that might result from lossy compression.

We start by first examining data from six LLM checkpoint sequences taken from Hugging Face (HF). We examine attributes of the data (type, shape, size, entropy) and how it evolves during the training process. This is followed by an evaluation of the effectiveness of applying common-of-the-shelf (COTS) compression engines. From an understanding of the data, in Section 4, we propose an alternative compression scheme based on Byte-Grouping (BG), Huffman Encoding and Run-Length Encoding (RLE) that offers more compressibility and reduced execution time than alternative COTS encoders. We evaluate our method and compare it with the best known alternatives.

## 2 Background: The Nature of LLM Tensors

Deep learning is a form of machine learning that builds large neural networks similar in essence to the human brain [5]. The neural network is composed of set of interconnected layers whereby artificial neurons "activate" according to an operation on their inputs. For dense networks, each neuron is connected to every other neuron of the next layer, hence its output value becomes the input for the next layer. During training, there are two neuron parameters that are adjusted: *weight* and *bias*. Weights are coefficients that affect the "strength" of each input ( $w_{ij} \cdot x_i$ ), that is, how much of the input data is fed into the activation function (see Figure 2). The weighted inputs are then summed and transformed using an activation function  $f$  to generate the output  $y_j$  as follows:

$$y_j = f\left(\sum (w_{ij} \cdot x_i) + b_j\right)$$

<sup>1</sup>An epoch is one full cycle through the input data

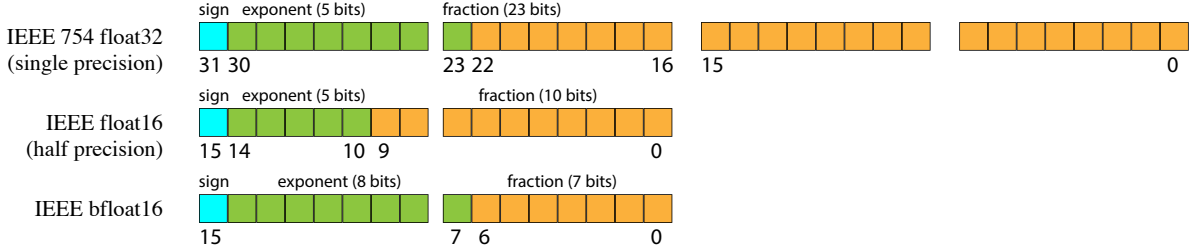


Figure 3: LLM Floating Point Formats

Name	Model Size (params)	Tokens	Type	Chkpt Size	Chkpt Count	Shard Splits
bloom	176B	366B	BF16	329GiB	20	72
amber	6.74B	1.25T	BF16	13GiB	358	3
transormer	7B	1.4T	BF16	28GiB	18	11
multibert	110M	160M	FP32	441MiB	28	1
olmo	7B	2.5T	FP32	26GiB	558	1
gpt2	124M	4M	FP32	1.4GiB	2000	1

Table 1: Attributes of Analyzed Data Sets

During the training phase of a neural network, weights and biases are adjusted iteratively to minimize the difference between the network’s predictions and the desired outcome. While LLM models and training is a complex matter outside the scope of this paper, these deep learning fundamentals carry through.

Neuron parameters are represented as numerical *tensors*. The term tensor is a generalisation of scalars and vectors. Tensor elements are floating point during training and often quantized to integer values for the purpose of inferencing.

**Floating-Point Representations** There are many bit representations of floating point numbers available in today’s computer systems. Most commonly, LLM models are based on one of three types: IEEE 32-bit float (single precision), IEEE 16-bit float (half precision) and Google’s 16-bit brain float [8] (see Figure 3). These formats differ by how many bits are available and how the bits are divided between the exponent and mantissa (also termed the fraction). Because most hardware now supports bfloat16 as a superior format for deep learning (performing nearly as well as float32 but using half the number of bits)[8], this paper focuses on the analysis of checkpointing data in float32 and bfloat16 formats (see Table 1).

### 3 Analysis of LLM Checkpoint Data

We examine checkpoint data for six different models that are all publicly available on Hugging Face (<https://huggingface.co/>). From these sources, we have analyzed over 28 TiB of tensor data. Three of the data sets are based on bfloat16 and three on float32. The attributes of the sample models are shown in Table 1. Additional information about the sample data is provided in Appendix A.

#### 3.1 Converging Behavior

As previously discussed, the purpose of training a model is to "tweak" the parameters until the optimum function of the neural network can be achieved. This adjustment of parameters lessens over time, eventually reaching values that are stable. Figure 4 shows a sample of weights (from shard `h.18.self_attention.dense.weight`) for the BLOOM data set. As is evident from the plot, at step 0 the values start randomly within the range  $\pm 0.005$ , then after a period of relatively aggressive change, they start to converge by around step 17. By step 20, the values are steady. This convergence behavior indicates that there are potential gains available for *delta encoding* between checkpoints.

We now examine the bit distribution, that is the ratio of zeros and ones. This data is from BLOOM and is therefore bfloat16. Figure 5 shows what proportion of bits (as a percentage on the z-axis) are set at that single point in time. Note that step 0 is at the rear of the plot, i.e., time runs from the back to the front.

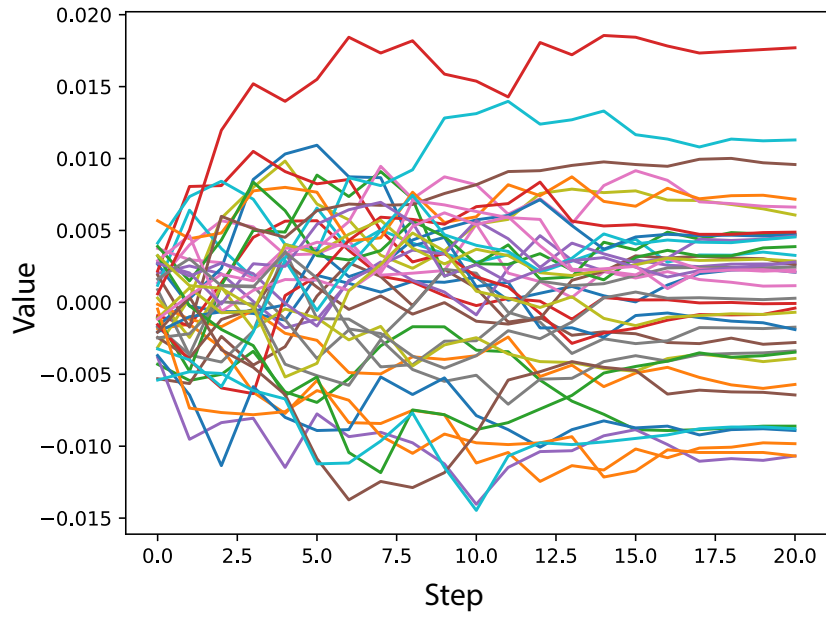


Figure 4: Sample Self-Attention Weights over Time from BLOOM Data Set

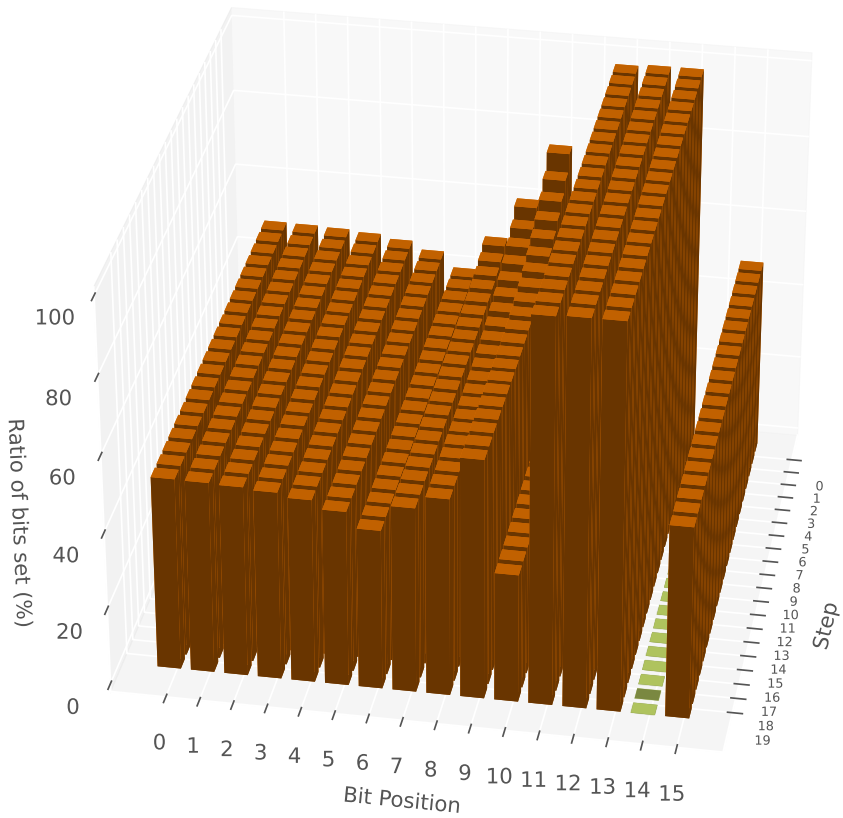


Figure 5: Bit Distribution for BLOOM Self-Attention QKV Weights Shard 0

Although the early steps are more volatile, the plot shows that most bits (except 10 and 14) flip between steps. Bit 14 is the most significant bit of the exponent (bit 15 is the sign bit) and is thus only set for values beyond the range of 7-bit exponent ( $3.4 * 10^{19}$ ,  $-3.4 * 10^{19} = 6.4 * 10^{19}$ ). In this data, the values are not reaching a magnitude to warrant this bit.

To explore further how tensor data changes over time, we examine how many bits are flipped between "steps" (refer to Figure 1), which represent an iteration of the whole input data set. We do this by examining the result of an XOR operation on values in step  $n$  and  $n + 1$ .

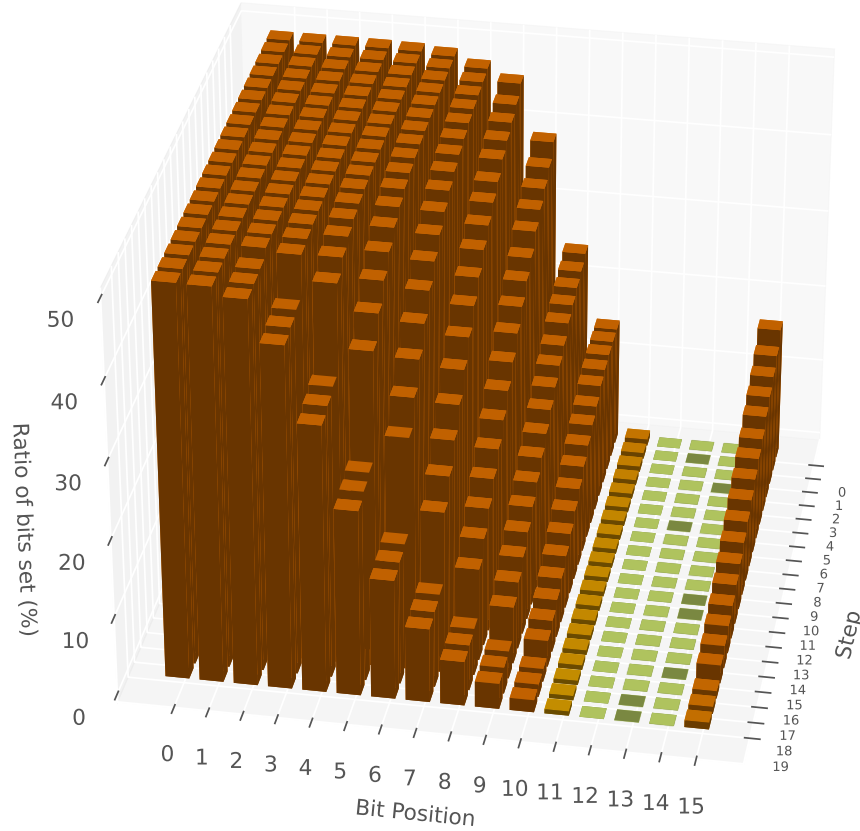


Figure 6: XOR Delta Bit Distribution for BLOOM Self-Attention QKV Weights Shard 0

Figure 6 shows the change in bit flip ratios as the step number increases. Note that step 0 is furthest back on the y-axis and that the z-axis maximum is 50% (i.e., equivalent to random change). This plot confirms several things. First, as indicated by falling bit set ratios (z-axis), stability increases as steps progress. Second, least-significant bits change more than most-significant bits - bits 10-14 rarely change at all. Third, sign bit changes reduce as the learning progresses, indicating less values are fluctuating across the zero boundary. In all, the "space available" in the three-dimensional cube suggest potential for compression.

While, Figure 6 shows increasing potential for compressability as learning progresses, it is clear that the lowest-significant bits (especially bits 0-4) continue to fluctuate even close to convergence. This is congruent with the nature of floating point representations. Figure 7 illustrates how bfloat16 bits change as 0.005 increments are made from -0.25 to 0.25. The yellow pixels indicate a bit flip (between the value and its incremented value). Bit 0 is at the top of the figure. From this figure, it is evident that even for very small increments, the first few bits almost always change.

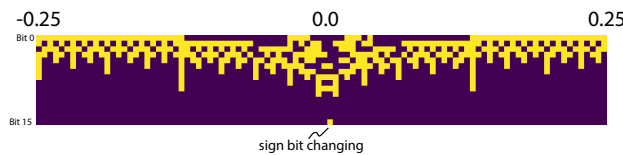


Figure 7: Bit changes for bfloat16 values -0.25 to 0.25 modified in 0.005 increments

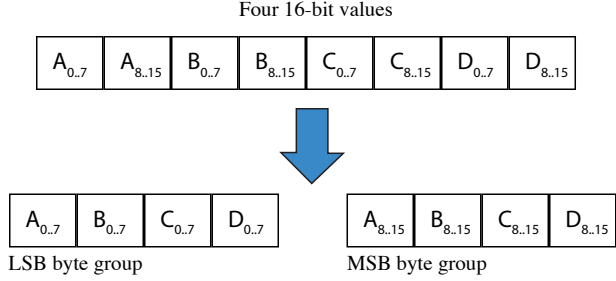


Figure 8: Example Byte-Grouping of four 16-bit values

## 4 Proposed Compression Algorithm

**Byte-Grouping and RLE** Byte-grouping (BG) is a simple modelling strategy that rearranges the data to exploit different stability across bytes. For example, considering Figure 6, the stability of the most-significant byte (bits 8-15) is much greater than the least-significant byte (bits 0-7). Byte-grouping copies bytes from their original position in the tensor value into contiguous regions of memory assigned to the group. For 16-bit values, two byte-groups are formed (see Figure 8 example). For 32-bit values, four byte-groups are formed.

Grouping more stable bytes in contiguous regions of memory, leads to more effective Run Length Encoding (RLE). RLE is a well known encoding method that replaces a symbol  $S$  with the pair  $(S, c)$  where  $c$  is the number of times  $S$  is repeated in this position. For example:

$$AAAABBBAACCC \rightarrow (A, 4), (B, 3), (A, 2), (C, 3)$$

Thus, RLE is effective when symbols are repeated. For the tensor delta data, repeating symbol zero is common and therefore RLE offers a path to additional compression.

### 4.1 Estimating compressibility with Entropy

Byte-grouping transformation seems to help many off-the-shelf compression engines so we are using this layout of data. Here we want to investigate what would be the compressibility of this type of data when using a simple model: considering bytes as independent compression symbols and measuring per symbol (byte) information content. The average amount of information per symbol over all alphabet (of 256 symbols) is known as the *entropy* of the symbols probability distribution and measured in bits is given by:

$$H = - \sum_{i=0}^{255} p_i \log_2 p_i$$

where  $p_i$  denotes the probability of occurrence of symbol  $i$  (byte value  $i$ ) of the alphabet. For a given probability distribution of the symbols, the entropy represents the minimum number of bits needed to represent a symbol without losing any information (i.e. the code to be uniquely decodable). Note that the worst case for the entropy is when the symbols are uniformly distributed, so the probability of each symbol is  $p_i = 1/256$  and the entropy  $H = 8$  bits.

To capture the changes in symbols probability distribution we provide *adaptivity* by computing symbols probability distribution on relatively small blocks of maximum  $64KiB$  (instead of entire file). As symbol probability  $p_i$  we use:

$$p_i = \frac{\text{number of occurrences of the symbol } i \text{ in the block}}{\text{block size in bytes}}$$

Figure 9 compares the compression ratios achieved by BZ2, DEFLATE and LZ4 (common off-the-shelf) with that which could be achieved by an entropy-based compression approach. BZ2 compression algorithm comes closer to the entropy, but it involves complex modelling by preprocessing data using the Burrows-Wheeler transform [2] making it quite slow.

Next, we examine an alternative entropy coder implementation that achieves the code size per symbol (byte) closer to entropy.

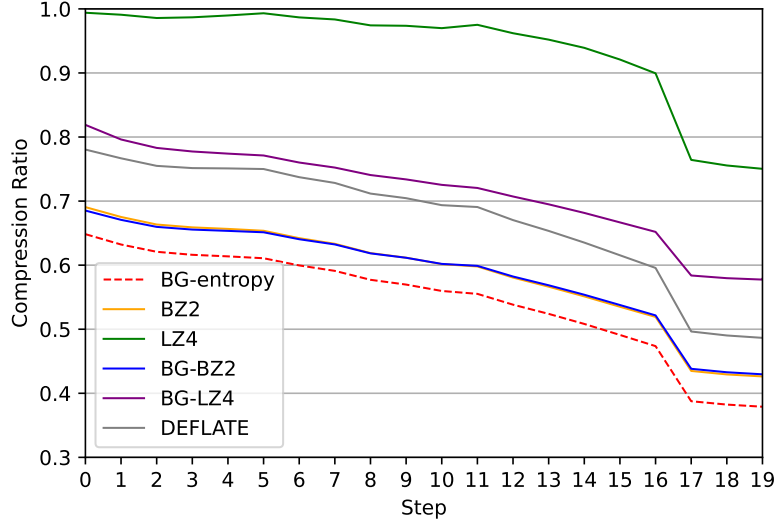


Figure 9: Entropy Comparison with Off-the-shelf Engines on BLOOM Data

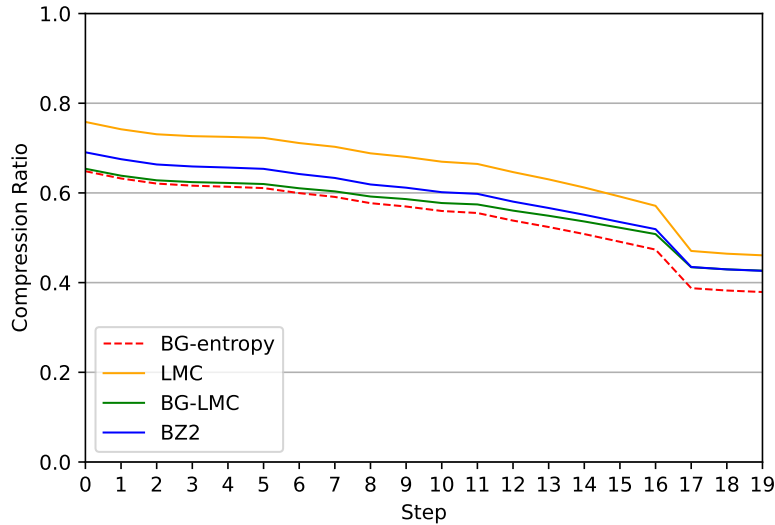


Figure 10: Comparison of BZ2, LMC, BG-LMC compression ratios vs. entropy of BLOOM data

## 4.2 Large Model Compression (LMC)

We investigate using a Huffman-based entropy encoder because it is fast and optimal within 1 bit of entropy. A somewhat better alternative (in terms of compression ratio) would be an arithmetic coder. However, arithmetic encoding is generally much slower than Huffman encoding. To adapt to changes in per byte statistics as for entropy estimation, we eventually compute a new Huffman codebook for each block of maximum  $64KB$  and encode it in compressed stream (similar to [3], [1]). Additionally, if the entire block consists of one byte value  $S$  repeated, it is encoded as a pair  $(S, c)$ , as in paragraph 4. In short, LMC compression scheme can be summarized as block adaptive Huffman coding + RLE. Figure 10 compares BG-LMC with BG-entropy showing that BG-LMC comes very close to the ideal compression ratio offered by the entropy. The data shows that as the input becomes more compressible, the entropy ratio becomes more difficult to achieve due to the use of integral bits/byte inherent to Huffman coding.

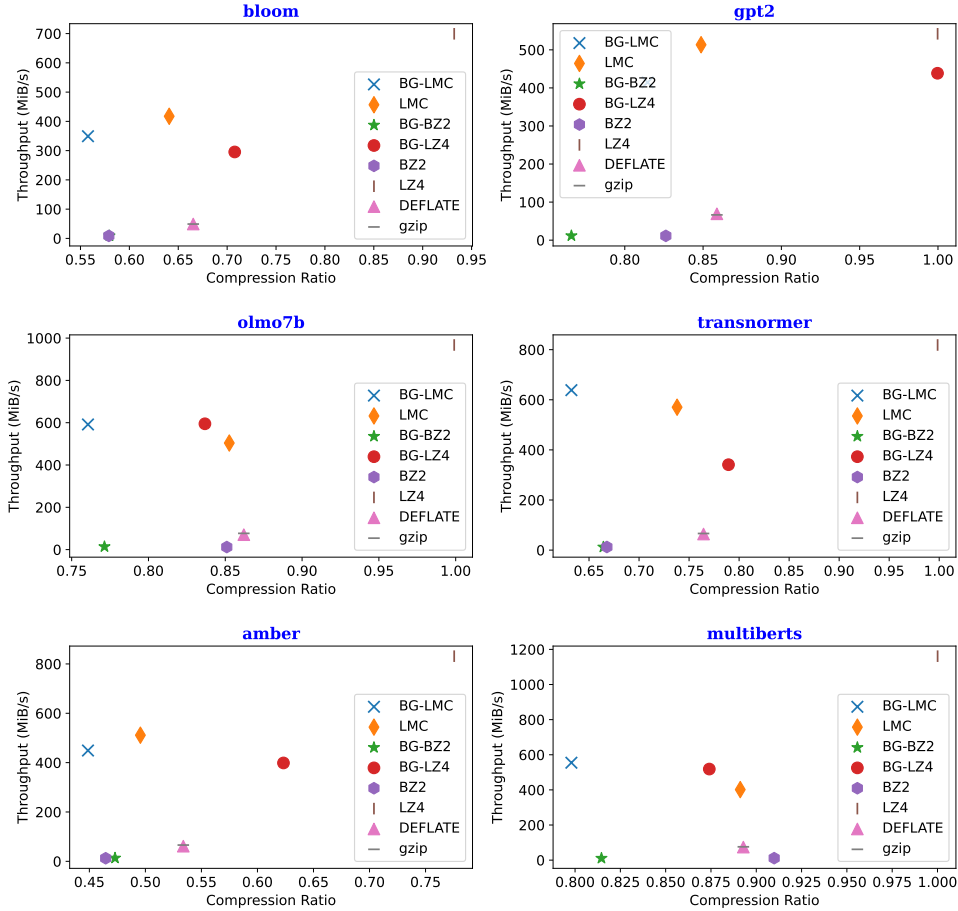


Figure 11: Summary of Encoder Performance

### 4.3 Parallel LMC (PLMC)

We implemented a simple data-parallel version of the BG-LMC algorithm (referred to as PLMC) that iteratively reads byte-grouped data into an input buffer and uses OpenMP to implement multi-threaded compression and decompression. The number of segments corresponds to the number of threads and is included in the codestream metadata, together with the compressed size of each piece. The implementation uses a default buffer size of 128 MiB. Nevertheless, this can be configured.

## 5 Experimental Results

The system used to collect the data is based on an AMD Epyc 7343 16-core processor with 512GiB main memory and 23TiB NVMe SSD.

### 5.1 Single-threaded Performance

**Compression Ratios and Processing Time** We collected data for compression ratio, compression throughput and decompression throughput. To better abstract the data, we calculated mean values across shard-deltas belonging to each data source. The primary attributes for consideration are compression ratio and throughput. For our use-case, compression performance is more important than decompression performance because the latter only happens in the event of disaster-recovery.

Figure 11 plots mean compression ratio vs. compression throughput for each of the six compression engines. The plots indicate that BG-LMC performs consistently better than the others. While BG-BZ2 achieves compression ratios within a few percent of BG-LMC its compression throughput performance is an order of magnitude slower. On the other end

of the spectrum, the data shows that LZ4 is typically the fastest to compress, but offers a relatively poor compression ratio - the best achieved being only 0.77 for the **amber** data set.

Appendix 3 shows data for decompression for a sample of five shards. BG-LMC decompression is 1.4x slower than the fastest decompression (LZ4).

**Compression Variance Over Time** We next examine how the compressability changes over time. As previously discussed, as convergence occurs the tensor values stabilize and thus the delta changes reduce - resulting in more zeros and therefore more compressability.

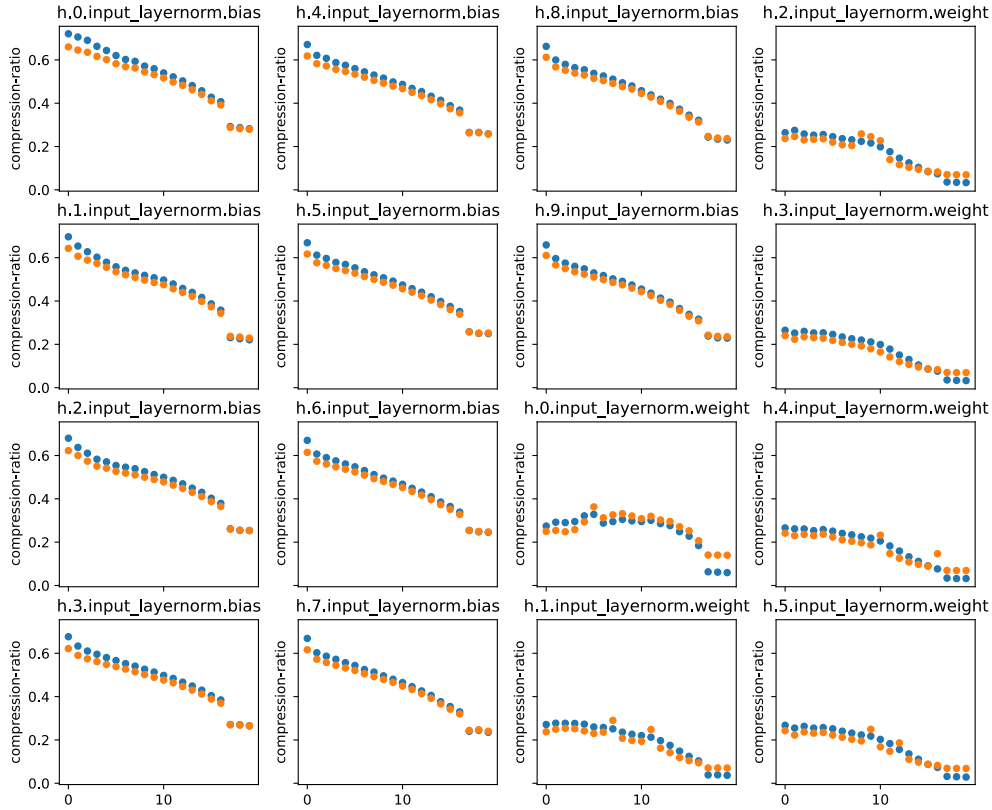


Figure 12: Compressability over time for 16 BLOOM shards  
Orange:BG-LMC, Blue:BZ2

Figure 12 shows how compressibility of shard-deltas changes over time for 16 samples (mixed weights and biases). We show data for BG-LMC and BZ2. In this sample, the compression ratio for biases changes from  $\sim 0.7$  to  $\sim 0.2$  and for weights changes from  $\sim 0.4$  to less than 0.1. As the data converges, the compressibility gradient flattens out.

## 5.2 Multi-core Scale-up Performance

To evaluate throughput scale-up, we evaluated concurrent implementations of LMC, GZIP and BZ2 - all on top of byte-grouped (BG) data. For these measurements IO bottlenecks were greatly reduced by using a RAM-disk. We chose a buffer size of 128 MiB although we found that throughput is not sensitive to buffer size. Figure 13 compares the compression throughput for the PLMC and off-the-shelf parallel implementations PIGZ and PBZ2. Figure 14 compares the decompression throughput. The compression ratio achieved by PLMC is 0.597 exceeding PIGZ (0.623) and PBZ2 (0.628) but with a significantly higher throughput. The data shows that compression scales relatively well for all three encoders. PIGZ decompression does not scale well.

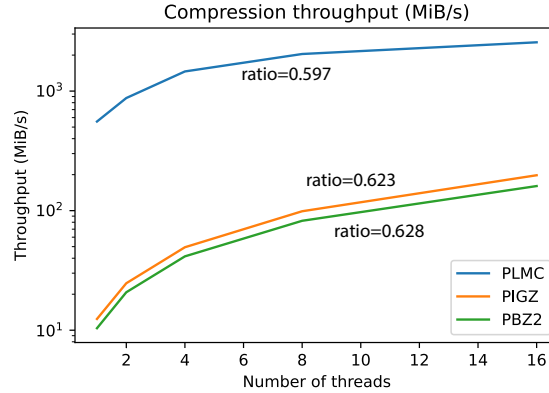


Figure 13: Comparison of PBZ2, PIGZ, PLMC compression throughput

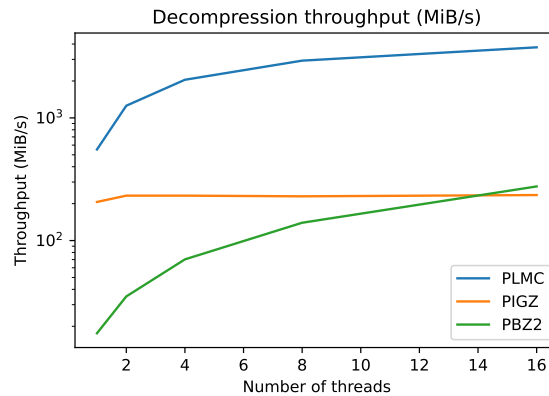


Figure 14: Comparison of PBZ2, PIGZ, PLMC decompression throughput (MiB/s)

## 6 Related Work

As a general survey [19] presents compression algorithms for language models, including lossy-based solutions such as quantization and parameter sharing. Although LLM tensor data is not covered, [17] presents analysis and benchmarking of lossless compression for floating-point data.

Prior work [18] has also explored the use of byte-grouping for tensor data for storage purposes. They do not cover incremental deltas nor improve on existing compression engines. Finally, [14] presents a general survey of time-series compression including work on combining Huffman encoding with delta and RLE [7].

## 7 Conclusions

In this paper we have explored the compressability of LLM tensor data for incremental snapshotting to storage. We examine how the tensor-deltas evolve over time down, how they are represented and how individual bits behave. With this knowledge in hand, we determined that entropy-based compression using Huffman encoding offers a superior solution to well known generic alternatives such as BZ2 and LZ4.

Our solution, BG-LMC, combines fast-modelling (byte-grouping and RLE) with Huffman encoding to achieve compression levels marginally better than the best off-the-shelf alternative (BZ2) but with an order of magnitude reduction in time-to-compress. This analysis shows using BG-LMC can achieve compression ratios of less than 0.6 and single-threaded compression throughput of  $\sim 300$  MB/s. For multi-core scale-up, our solution achieves performance beyond parallel implementations of gzip and BZ2, attaining over 2.5GiB/s and 3.6GiB/s for compression and decompression respectively on only 16 cores.

## References

- [1] Daniel S. Hirschberg and Debra A. Lelewer. “Efficient Decoding of Prefix Codes”. In: *Communications of the ACM* 33 (1990), pp. 449–459.
- [2] Michael Burrows and David J. Wheeler. *A Block-Sorting Lossless Data Compression Algorithm*. Tech. rep. 124. Digital Systems Research Center, May 1994.
- [3] L. Peter Deutsch. *DEFLATE Compressed Data Format Specification version 1.3*. RFC 1951. May 1996. DOI: 10.17487/RFC1951. URL: <https://www.rfc-editor.org/info/rfc1951>.
- [4] Catello Di Martino et al. “Lessons Learned from the Analysis of System Failures at Petascale: The Case of Blue Waters”. In: *2014 44th Annual IEEE/IFIP International Conference on Dependable Systems and Networks*. 2014, pp. 610–621. DOI: 10.1109/DSN.2014.62.
- [5] Nikhil Buduma and Nicholas Locascio. *Fundamentals of Deep Learning: Designing Next-Generation Machine Intelligence Algorithms*. 1st. O’Reilly Media, Inc., 2017. ISBN: 1491925612.
- [6] Saurabh Gupta et al. “Failures in large scale systems: long-term measurement, analysis, and implications”. In: *Proceedings of the International Conference for High Performance Computing, Networking, Storage and Analysis*. SC ’17. Denver, Colorado: Association for Computing Machinery, 2017. ISBN: 9781450351140. DOI: 10.1145/3126908.3126937. URL: <https://doi.org/10.1145/3126908.3126937>.
- [7] Hussein Sh. Mogahed and Alexey G. Yakunin. “Development of a Lossless Data Compression Algorithm for Multichannel Environmental Monitoring Systems”. In: *2018 XIV International Scientific-Technical Conference on Actual Problems of Electronics Instrument Engineering (APEIE)*. 2018, pp. 483–486. DOI: 10.1109/APEIE.2018.8546121.
- [8] Neil Burgess et al. “Bfloat16 Processing for Neural Networks”. In: *2019 IEEE 26th Symposium on Computer Arithmetic (ARITH)*. 2019, pp. 88–91. DOI: 10.1109/ARITH.2019.00022.
- [9] Tom B. Brown et al. *Language Models are Few-Shot Learners*. 2020. arXiv: 2005.14165 [cs.CL]. URL: <https://arxiv.org/abs/2005.14165>.
- [10] Kiwan Maeng et al. *CPR: Understanding and Improving Failure Tolerant Training for Deep Learning Recommendation with Partial Recovery*. 2020. arXiv: 2011.02999 [cs.LG]. URL: <https://arxiv.org/abs/2011.02999>.
- [11] Jayashree Mohan, Amar Phanishayee, and Vijay Chidambaram. “CheckFreq: Frequent, Fine-Grained DNN Checkpointing”. In: *19th USENIX Conference on File and Storage Technologies (FAST 21)*. USENIX Association, Feb. 2021, pp. 203–216. ISBN: 978-1-939133-20-5. URL: <https://www.usenix.org/conference/fast21/presentation/mohan>.
- [12] Thibault Sellam et al. “The MultiBERTs: BERT Reproductions for Robustness Analysis”. In: *CoRR* abs/2106.16163 (2021). arXiv: 2106.16163. URL: <https://arxiv.org/abs/2106.16163>.

- [13] Assaf Eisenman et al. “Check-N-Run: a Checkpointing System for Training Deep Learning Recommendation Models”. In: *19th USENIX Symposium on Networked Systems Design and Implementation (NSDI 22)*. Renton, WA: USENIX Association, Apr. 2022, pp. 929–943. ISBN: 978-1-939133-27-4. URL: <https://www.usenix.org/conference/nsdi22/presentation/eisenman>.
- [14] Giacomo Chiarot and Claudio Silvestri. “Time Series Compression Survey”. In: *ACM Comput. Surv.* 55.10 (Feb. 2023). ISSN: 0360-0300. DOI: 10.1145/3560814. URL: <https://doi.org/10.1145/3560814>.
- [15] Zhuang Wang et al. “GEMINI: Fast Failure Recovery in Distributed Training with In-Memory Checkpoints”. In: *Proceedings of the 29th Symposium on Operating Systems Principles. SOSP ’23*. Koblenz, Germany: Association for Computing Machinery, 2023, pp. 364–381. ISBN: 9798400702297. DOI: 10.1145/3600006.3613145. URL: <https://doi.org/10.1145/3600006.3613145>.
- [16] BigScience Workshop et al. *BLOOM: A 176B-Parameter Open-Access Multilingual Language Model*. 2023. arXiv: 2211.05100 [cs.CL].
- [17] Xinyu Chen et al. “FCBench: Cross-Domain Benchmarking of Lossless Compression for Floating-Point Data”. In: *Proc. VLDB Endow.* 17.6 (May 2024), pp. 1418–1431. ISSN: 2150-8097. DOI: 10.14778/3648160.3648180. URL: <https://doi.org/10.14778/3648160.3648180>.
- [18] Moshik Hershcovitch et al. *Lossless and Near-Lossless Compression for Foundation Models*. 2024. arXiv: 2404.15198 [cs.LG]. URL: <https://arxiv.org/abs/2404.15198>.
- [19] Seungcheol Park et al. *A Comprehensive Survey of Compression Algorithms for Language Models*. 2024. arXiv: 2401.15347 [cs.CL]. URL: <https://arxiv.org/abs/2401.15347>.

## Appendix A

### A.1 Data Set Descriptions

- **Bloom** - BigScience Large Open-science Open-access Multilingual Language Model (BLOOM) [16]  
<https://huggingface.co/bigscience/bloom>.
- **Amber** - Amber is a 7B English language model using the LLaMA architecture.  
<https://huggingface.co/LLM360/Amber>
- **Transnormer** - Linear transformer aimed at reducing the quadratic space-time complexity of vanilla transformers. TransNormerLLM is the first linear attention-based LLM that outperforms conventional softmax attention-based models in terms of both accuracy and efficiency.  
<https://huggingface.co/OpenNLPLab/TransNormerLLM-7B>
- **Olmo** - OLMo is a series of Open Language Models designed to enable the science of language models. The OLMo models are trained on the Dolma dataset.  
<https://huggingface.co/allenai/OLMo-7B>
- **Multiberts** - MultiBERTs (pretrained BERT) model on English language using a masked language modeling (MLM) objective. The model is based on the paper by Sellam et al. [12].  
<https://huggingface.co/MultiBertGunjanPatrick/multiberts-seed-0>
- **Gpt2** - A reproduction of GPT-2 based on 124M parameters trained using x8 A100 GPUs on OpenWebText.  
<https://github.com/karpathy/nanoGPT>

### A.2 Tensor Dimensions for Sample Data

Bloom	Amber	Transnormer	Multiberts	Olmo	GPT2
14336 (425)	32000 x 4096 (2)	5120 (44)	512 x 512 (1)	50304 x 4096 (2)	1024 x 768 (1)
43008 x 14336 (70)	4096 (65)	5120 x 5120 (42)	30522 x 768 (2)	12288 x 4096 (32)	50257 x 768 (1)
43008 (70)	4096 x 4096 (128)	5120 x 15360 (42)	512 x 768 (1)	4096 x 4096 (32)	1024 x 1024 (12)
14336 x 14336 (70)	11008 x 4096 (64)	15360 x 5120 (126)	1536 x 768 (2)	4096 x 11008 (32)	2304 (12)
57344 x 4336 (70)	4096 x 11008 (32)	5120 x 15360 (42)	768 (114)	22016 x 4096 (32)	768 x 2304 (12)
57344 (70)				768 x 768 (50)	768 (74)

Table 2: Tensor shard shapes for analyzed data sets (count in parenthesis)

## A.3 Detailed Results for BLOOM Data Set

Encoder	Shard	Mean Compression Ratio	Shard Size	Mean Encode Time (seconds)	Mean Decode Time (seconds)	Steps
BG-LMC	h.X.mlp.dense_4h_to_h.weight	0.565	1.5GiB	4.6762	4.5397	200
BG-LMC	h.X.mlp.dense_h_to_4h.weight	0.530	1.5GiB	4.7379	4.6953	200
BG-LMC	h.X.self_attention.dense.weight	0.600	392.0MiB	1.0748	1.0068	200
BG-LMC	h.X.self_attention.query_key_value.weight	0.519	1.1GiB	3.4900	3.3678	200
BG-LMC	word_embeddings.weight	0.574	6.7GiB	23.5087	24.0144	20
LMC	h.X.mlp.dense_4h_to_h.weight	0.647	1.5GiB	3.6747	3.1807	200
LMC	h.X.mlp.dense_h_to_4h.weight	0.603	1.5GiB	3.6340	3.2266	200
LMC	h.X.self_attention.dense.weight	0.695	392.0MiB	0.9288	0.8136	200
LMC	h.X.self_attention.query_key_value.weight	0.594	1.1GiB	2.7130	2.3578	200
LMC	word_embeddings.weight	0.664	6.7GiB	17.0775	16.1114	20
BG-BZ2	h.X.mlp.dense_4h_to_h.weight	0.593	1.5GiB	154.3418	79.0762	200
BG-BZ2	h.X.mlp.dense_h_to_4h.weight	0.542	1.5GiB	137.3355	72.3389	200
BG-BZ2	h.X.self_attention.dense.weight	0.627	392.0MiB	41.7933	20.6631	200
BG-BZ2	h.X.self_attention.query_key_value.weight	0.538	1.1GiB	103.2792	54.1697	200
BG-BZ2	word_embeddings.weight	0.599	6.7GiB	673.7042	344.8112	20
BG-LZ4	h.X.mlp.dense_4h_to_h.weight	0.722	1.5GiB	4.3664	1.6828	200
BG-LZ4	h.X.mlp.dense_h_to_4h.weight	0.669	1.5GiB	4.0569	1.6928	200
BG-LZ4	h.X.self_attention.dense.weight	0.754	392.0MiB	1.1768	0.4081	200
BG-LZ4	h.X.self_attention.query_key_value.weight	0.670	1.1GiB	3.1123	1.3113	200
BG-LZ4	word_embeddings.weight	0.725	6.7GiB	21.4897	9.5665	20
BZ2	h.X.mlp.dense_4h_to_h.weight	0.593	1.5GiB	171.0602	85.7883	200
BZ2	h.X.mlp.dense_h_to_4h.weight	0.543	1.5GiB	157.7029	79.5812	200
BZ2	h.X.self_attention.dense.weight	0.627	392.0MiB	43.2183	21.4598	200
BZ2	h.X.self_attention.query_key_value.weight	0.535	1.1GiB	117.3340	60.5858	200
BZ2	word_embeddings.weight	0.598	6.7GiB	734.9330	371.4208	20
LZ4	h.X.mlp.dense_4h_to_h.weight	0.948	1.5GiB	3.2303	1.3582	200
LZ4	h.X.mlp.dense_h_to_4h.weight	0.888	1.5GiB	3.7749	1.5014	200
LZ4	h.X.self_attention.dense.weight	0.976	392.0MiB	0.6223	0.3190	200
LZ4	h.X.self_attention.query_key_value.weight	0.885	1.1GiB	2.8173	1.1237	200
LZ4	word_embeddings.weight	0.964	6.7GiB	14.3532	7.8359	20
DEFLATE	h.X.mlp.dense_4h_to_h.weight	0.679	1.5GiB	34.7788	18.3078	200
DEFLATE	h.X.mlp.dense_h_to_4h.weight	0.619	1.5GiB	35.0574	16.4662	200
DEFLATE	h.X.self_attention.dense.weight	0.722	392.0MiB	8.2072	4.8629	200
DEFLATE	h.X.self_attention.query_key_value.weight	0.616	1.1GiB	26.7587	12.4380	200
DEFLATE	word_embeddings.weight	0.691	6.7GiB	145.9071	81.3236	20
gzip	h.X.mlp.dense_4h_to_h.weight	0.679	1.5GiB	35.0080	18.5110	200
gzip	h.X.mlp.dense_h_to_4h.weight	0.619	1.5GiB	34.9759	16.5045	200
gzip	h.X.self_attention.dense.weight	0.722	392.0MiB	8.1997	4.8827	200
gzip	h.X.self_attention.query_key_value.weight	0.616	1.1GiB	26.7039	12.5117	200
gzip	word_embeddings.weight	0.691	6.7GiB	145.7747	82.2829	20